Collective Behavior of a Population of Chemically Coupled Oscillators

Rita Toth,[†] Annette F. Taylor,*[,†] and Mark R. Tinsley[‡]

Department of Chemistry, University of Leeds, Leeds, LS2 9JT, U.K., and Department of Chemistry, West Virginia University, Morgantown, West Virginia 26506

Received: February 3, 2006; In Final Form: March 20, 2006

Experiments are performed in which a large number ($\sim 10^4$) of relaxation oscillators are globally coupled through the concentration of chemicals in the surrounding solution. Each oscillator consists of a microscopic catalyst-loaded particle that displays oscillations in the concentrations of chemical species when suspended in catalyst-free Belousov−Zhabotinsky (BZ) reaction solution. In the absence of stirring, the uncoupled particles display a range of oscillatory frequencies. In the well-stirred system, oscillations appear in the surrounding solution for greater than a critical number density of particles (n_{crit}). There is a growth in the amplitude of oscillations with increasing n, accompanied by a slight increase or no change in frequency. A model is proposed to account for the behavior, in which the transfer of activator and inhibitor to and from the bulk medium is considered for each particle. We demonstrate that the appearance and subsequent growth in the amplitude of oscillations may be associated with partial synchronization of the oscillators.

Introduction

Many physical, chemical, and biological systems might be considered as coupled individual oscillating elements.[1] Such systems undergo transitions in their collective behavior arising from interactions between elements. Possibly the simplest response in a population of coupled oscillators is that of frequency and/or phase synchronization.[2,3] The theory of synchronization of biological oscillators such as fireflies,[4] yeast cells,[5] heart cells,[6] and neurons[7] has inspired scientists from all disciplines for decades since the pioneering theoretical work of Winfree[8] and Kuramoto.[9] The Kuramoto transition to synchronization is characterized by a sigmoid growth in the collective amplitude of the oscillators, where for less than a critical coupling strength the oscillators are phase randomized and only noise is observed in the collective signal, then, following the appearance of oscillations, the oscillators rapidly align. Such a transition requires the application of global (all-to-all) coupling.

Global coupling occurs when each oscillator is connected to every other through, for example, the concentrations of a chemical in an external medium and is believed to be responsible for the synchronization of a variety of biological oscillators. Suspensions of the amoebae *Dictyostelium discoideum* synchronously emit cAMP if the cell density (the number of cells per unit volume of extracellular solution) is sufficient.[10] The macroscopic glycolytic oscillations observed in suspensions of yeast cells last longer for higher cell densities, and there has been evidence to suggest that these independent oscillators synchronize through exchange of acetaldehyde with the extracellular medium.[11,12] It is well-known that networks of neurons can display synchronous activity associated with both healthy and pathological functioning.[13,14] Models of such behavior generally include fast local as well as nonlocal connectivity between neurons, but it has also been demonstrated that synchronization is possible in groups of neurons globally connected through the level of a neurotransmitter, provided the spatial transfer of the neurotransmitter is fast compared with the time scale of the oscillations.[15]

Experimental investigations of globally coupled chemical oscillators have been illuminating but are mainly limited to small numbers of oscillators or include additional local coupling. The response of up to 16 electrically or chemically coupled continuous stirred tank reactors (CSTRs) has been investigated with the observations of synchronization and other phenomenon such as oscillator death or chaos.[16−19] Global coupling in a spatially distributed Belousov−Zhabotinsky (BZ) reaction was achieved through the use of light; in this case, cluster patterns were observed, as well as bulk oscillations.[20] Similar phenomena have been observed in the oxidation of CO on Pt, coupled through the gas phase.[21] The first well-characterized experimental example of a Kuramoto-type transition to synchronization was recently demonstrated in 64 electrochemical oscillators globally coupled through a common load.[22] This experimental setup has the distinct advantage of controllable and observable individual oscillator dynamics. In a series of papers, Kiss, Hudson, and others have examined how the transition is affected by the oscillator dynamics, finite population size, and degree of heterogeneity of the population, as well as associated phenomena such as frequency clustering.[23−26] There are still comparatively few experimental studies of these phenomena, compared with the wealth of theoretical and numerical investigations.[27]

In this paper, we examine an experimental system in which a large number ($\sim 10^4$) of relaxation oscillators are coupled through the concentration of chemicals in the surrounding solution. The oscillators consist of catalytic particles for the BZ reaction suspended catalyst-free solution. No oscillations are possible in the surrounding solution in the absence of the catalyst particles. In an unstirred reactor, the particles are monitored spectrophotometrically and display a range of oscillatory frequencies. In the well-stirred reactor, we follow the redox potential of the reaction solution and observe the appearance

* To whom correspondence should be addressed. E-mail: A. F.Taylor@leeds.ac.uk.
[†] University of Leeds.
[‡] West Virginia University.

10.1021/jp060732z CCC: $33.50
Published on Web 05/03/2006

TABLE 1: Experimental Parameter Values ($A = [NaBrO_3]_0$, $B = [CH_3(COOH)_2]_0$, $H = [H_2SO_4]_0$, $D = [NaBr]_0$, Particle 1 = DOWEX 50WX4-200, Particle 2 = DOWEX 50WX4-50, and V is the volume displacement of 1 g of particles in water)

	A/M	*B*/M	*H*/M	*D*/M	particle	V/cm^3 g^{-1}	$\langle r_i \rangle$/cm
A	0.49	0.14	0.67	0.07	1	0.96	0.010
B	0.49	0.14	1.00	0.07	1	0.96	0.010
C	0.49	0.14	0.67	0.07	2	0.86	0.035

of oscillations for a critical number density of particles (n_{crit}) that depends on the composition of the solution and the particle size. The frequency of the signal is constant or slightly increases with the number density. The transition is investigated in a model which incorporates the BZ reaction for each particle and the transfer of species into the bulk solution. We assume the stirring is sufficient to maintain the concentrations of the chemicals in solution spatially homogeneous, and hence, the particles may be considered as globally coupled. We find that the appearance of oscillations in the solution and subsequent growth in amplitude may be associated with the partial synchronization of the individual oscillators. A small fraction of the oscillators are forced by the global signal and exhibit complex oscillations. We also investigate the transition for higher exchange rates and find a sudden transition to the fully synchronized state. In this case, the synchronization frequency is much lower than that of the uncoupled state and decreases with increasing *n*.

Experimental Section

We used porous cation-exchange particles (DOWEX) which were loaded with catalyst for the Belousov−Zhabotinsky (BZ) reaction by stirring in ferroin solution overnight ([ferroin] = 1.7×10^{-5} mol/g particles). The particles were then washed with distilled water and 0.1 M sulfuric acid solution and left to dry in air for 24 h. Catalyst-loaded particles are known to display relaxation oscillations with a range of frequencies when placed in catalyst-free BZ solution.[28,29]

We exploited three different experimental compositions as listed in Table 1: composition A, composition B with higher sulfuric acid concentration, and composition C with a larger average particle size. To determine the natural frequency distribution of the oscillators, a small number of particles were suspended in 10 cm^3 of catalyst-free BZ solution in a petri dish. The change between the blue and red colors of the catalyst due to the redox reaction was monitored every third second with a CCD camera attached to a microscope. The recorded color change was transformed to a light intensity change with Image-Pro Plus imaging system. The intensity was obtained by averaging the gray level of a fixed small area. Determination of frequency involved particles sufficiently spaced such that local (diffusional) coupling could be ignored. We also determined the average radius of a bead, $\langle r_i \rangle$, for a particular sample as purchased.

The collective behavior of the oscillators was monitored by adding a certain mass of catalyst-loaded beads into 10 cm^3 of freshly prepared catalyst-free BZ solution in a stirred tank reactor. The solution was stirred with a magnetic stirrer at a constant rate (600 rpm) chosen to maintain a homogeneous distribution of particles within the reactor. Hydrodynamic instabilities are not believed to contribute to the behavior described in this work as the mixing time scale is much shorter (∼1 s) than that of the chemical relaxation time scale (∼40 s).[30,31] The amplitude of oscillations was recorded through the redox potential measured every second with a combination electrode. It is likely that the combination electrode mainly follows the bromine-containing redox couples in solution, rather than the change in oxidation state of the catalyst on the particles (see Figure 2). We estimate the number density of particles, *n*, from

$$n = \frac{N}{V_s} = \frac{V}{\langle V_i \rangle V_s} \tag{1}$$

where N is the number of particles in the total volume of solution V_s (= 10 cm^3), V is the volume displacement of the mass of particles added to solution, and $\langle V_i \rangle$ is the average volume of a particle calculated from $\langle r_i \rangle$ (Table 1). The potential was recorded until any initial transient converted to stable behavior. The amplitude of the oscillations was then determined as an average over several oscillations.

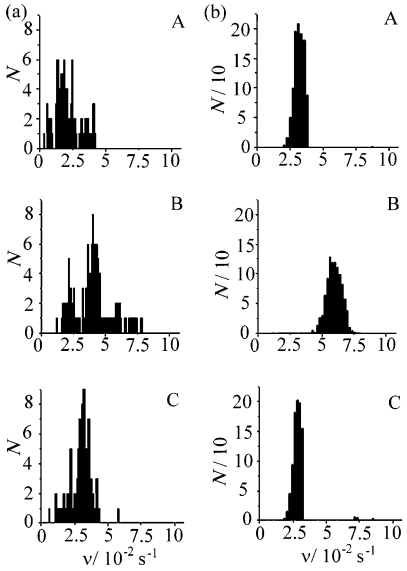

Figure 1. Experimental frequency distribution of ∼150 chemical oscillators with compositions A, B, and C (column a) and simulated frequency distribution of 1000 oscillators with compositions A, B, and C (column b).

TABLE 2: Average Oscillatory Frequencies and Critical Number Densities (i = unstirred and s = stirred)

	experimental			numerical		
	$\langle \upsilon_i \rangle$/s^{-1}	$\langle \upsilon_s \rangle$/s^{-1}	n_{crit}/cm^{-3}	$\langle \upsilon_i \rangle$/s^{-1}	$\langle \upsilon_s \rangle$/s^{-1}	n_{crit}/cm^{-3}
A	0.024	0.035	5000	0.028	0.028	5000
B	0.04	0.053	7000	0.059	0.062	11000
C	0.032	0.042	400	0.030	0.030	500

Results

The frequency distribution of the individual chemical oscillators in the unstirred reactor is shown in Figure 1 for the different experimental conditions listed in Table 1, rows A, B, and C. We verified that the particles displayed oscillations in the unstirred reactor for the masses exploited in the well-stirred reactor and that the beads continued to oscillate with a range of frequencies following stirring. The mean frequencies in the unstirred reactor are listed in Table 2.

Figure 2 shows a typical potential−time series for four experiments in the well-stirred reactor with an increasing number density of particles, *n*. For low numbers of particles, the trace shows only noise. Oscillations appear in the bulk solution for greater than a certain value of *n*. There is a time delay between the start of the reaction and the appearance of oscillations, the

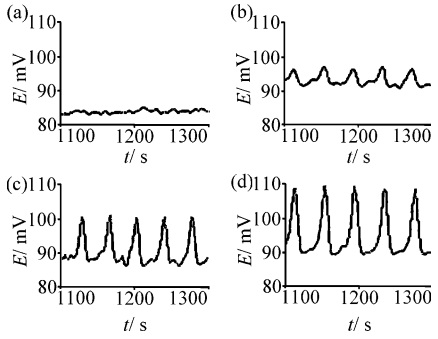

Figure 2. Temporal evolution of oscillations in potential (E) in the well-stirred reactor for composition A with an increasing estimated number density of particles: (a) $n = 2000$ cm^{-3}, (b) $n = 5000$ cm^{-3}, (c) $n = 7000$ cm^{-3}, and (d) $n = 10\,000$ cm^{-3}.

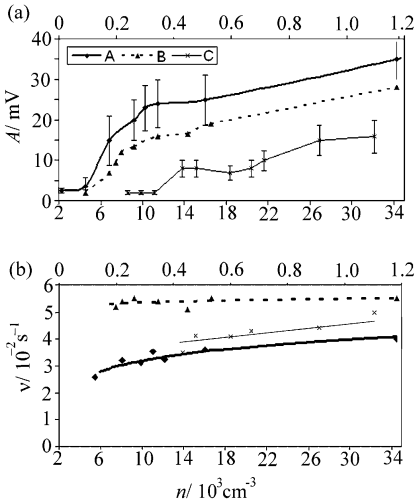

Figure 3. (a) Amplitude and (b) frequency of oscillations in potential with an estimated number density of particles in the well-stirred reactor with compositions A, B, and C (the lower x-axis is for compositions A and B, and the upper x-axis is for composition C).

length of which increases with proximity to the critical n. The oscillations are broad, and there is some evidence of a small secondary peak between maxima.

The growth in amplitude of oscillations as a function of the number density of particles is shown in Figure 3a for the three different experimental compositions. The frequency of oscillations increases slightly with n for compositions A and C and is approximately constant for composition B (Figure 3b). The average values of the bulk oscillatory frequency are listed in Table 2. The amplitude of oscillations was determined as an average of several experimental runs, and there was a significant variation between runs. In all cases for n less than a critical amount, only noise was observed, and greater than the critical amount, the amplitude of oscillations increased with increasing n. The appearance of oscillations can be clearly distinguished from noise from a Fourier analysis of the time series, and the approximate values of n_{crit} are listed in Table 2.

Model. The main processes in the model are the Belousov−Zhabotinsky (BZ) reaction, which takes place on each catalyst particle and the transfer of species between each particle and the surrounding catalyst-free BZ solution. A schematic of the model is shown in Figure 4. The kinetic equations for the activator species $HBrO_2$ (X), which catalyzes its own production, the inhibitor species Br^- (Y), and the oxidized form of the metal catalyst $Fe(phen)_3^{3+}$ (Z) are given by the ZBKE model of the BZ reaction.[32] We assume the concentrations of the reactants are in large excess compared with the intermediate species and

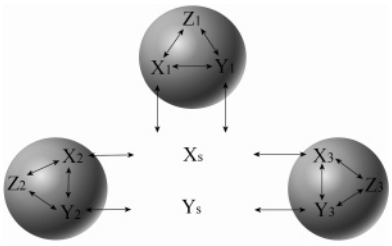

Figure 4. Schematic of processes included in the model where X_i, Y_i, and Z_i are the concentrations of $HBrO_2$, Br^-, and $Fe(phen)_3^{3+}$ for the ith particle and X_s and Y_s correspond to the concentration of $HBrO_2$ and Br^- in the surrounding solution.

do not change during the time we monitor the behavior. The model is reduced with appropriate scalings to the following set of equations (Appendix 1)

$$\frac{dx_i}{d\tau} = -k(x_i - x_s) + \frac{1}{\epsilon_1}(-x_i^2 - x_i + \epsilon_2\gamma u_{ss}^2 + u_{ss}(1 - z_i) - \delta x_i z_i + \mu y_i - x_i y_i) \quad (2)$$

$$\frac{dy_i}{d\tau} = -k(y_i - y_s) + \frac{1}{\epsilon_4}\left(-x_i y_i - \mu y_i + q\frac{\alpha z_i}{\epsilon_3 + 1 - z_i} + \beta\right) \quad (3)$$

$$\frac{dz_i}{d\tau} = u_{ss}(1 - z_i) - \delta x_i z_i - \frac{\alpha z_i}{\epsilon_3 + 1 - z_i} \quad (4)$$

$$\frac{dx_s}{d\tau} = \frac{nV_i}{N}\sum_{i=1}^{N} k(x_i - x_s) + \frac{1}{\epsilon_1}(-x_s^2 - x_s + \mu y_s - x_s y_s) \quad (5)$$

$$\frac{dy_s}{d\tau} = \frac{nV_i}{N}\sum_{i=1}^{N} k(y_i - y_s) + \frac{1}{\epsilon_4}(-x_s y_s - \mu y_s + \beta) \quad (6)$$

where x_i, y_i, and z_i, are the dimensionless $[HBrO_2]_i$, $[Br^-]_i$, and $[Fe(phen)_3^{3+}]_i$ for $i = 1,...,N$ particles and x_s and y_s are the dimensionless $[HBrO_2]_s$ and $[Br^-]_s$ in the surrounding solution. The dimensionless concentration of $HBrO_2^+$ (u_{ss}) is given by its steady-state value (Appendix 1). The parameters $\epsilon_1-\epsilon_4$, α, β, δ, γ, and μ are related to the reaction rate constants and initial concentrations, and k is the scaled coefficient for the net rate of transfer of $HBrO_2$ and Br^- into the surrounding solution. The rate equations for $HBrO_2$ and Br^- in the surrounding solution include the dilution factor nV_i/N ($= V_i/V_s$) where n is the number density of particles (N/V_s) as before. The value of n is increased by increasing N with fixed V_s ($= 10$ cm^3). A range of the particle natural frequencies is obtained by a Gaussian distribution in the value of q, the stoichiometric coefficient for the reaction, and the mean value of q was chosen to best reflect the experimentally determined frequencies. The value of k can be estimated from the scaling $\times\ k_{sl}A_i/V_i$, where k_{sl} is the particle−liquid mass transfer coefficient with units of length/time, A_i is the interfacial area between phases, and V_i is the characteristic reaction volume of a particle. Values of the particle−liquid mass transfer coefficient (k_{sl}) for porous particles in well-stirred reactors are of the order of $10^{-3}-10^{-1}$ cm s^{-1}, and the value depends on the particle size and stirring rate.[33] We fix the value of k_{sl} at 0.01 cm s^{-1}. Although the particles are open, porous structures, it is likely that the reaction itself will mainly take place at the surface of a particle, so an exact value of V_i cannot be determined. We take a value of $V_i = 2 \times 10^{-5}$ cm^3 for the smaller catalyst particles or 9×10^{-4} cm^3 for

TABLE 3: Numerical Parameter Values

	$\epsilon_1/10^{-1}$	$\epsilon_2/10^{-5}$	$\epsilon_3/10^{-3}$	$\epsilon_4/10^{-4}$	$\alpha/10^{-4}$	$\beta/10^{-4}$	$\gamma/10^{-1}$	$\delta/10^{-4}$	$\mu/10^{-4}$	$k/10^{-1}$	$(V_i/V_s)/10^{-6}$	$q/\pm0.05$
A	1.0	1.1	2.3	3.0	1.7	8.9	2.5	1.7	5.9	20	2.0	0.60
B	1.6	2.6	1.6	3.2	0.5	3.7	2.5	1.11	4.1	8.5	2.0	0.84
C	1.0	1.1	2.3	3.0	1.7	8.9	2.5	1.7	5.9	5.2	90	0.60

the larger particles. The calculated values of k and all other parameters used in simulations are listed in Table 3.

Model Results. The frequency distribution for uncoupled particles is obtained with a reduced value of k (k_{sl} is reduced by a factor of 5 relative to the stirred system), for the three different reaction compositions (Figure 1, column b). The mean frequencies are listed in Table 2. Typical oscillations in x_i, the dimensionless concentration of $HBrO_2$, on four different particles are shown in Figure 5, and each display the characteristic sharp growth of activator followed by a less rapid decay.

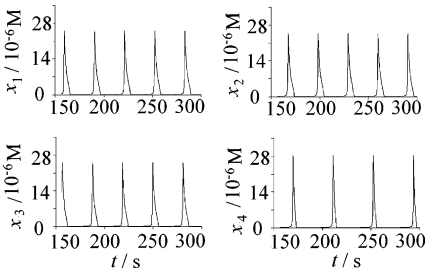

Figure 5. Simulated oscillations in the concentration of $HBrO_2$ on four different particles in the uncoupled system. Parameters are listed in Table 3, row A.

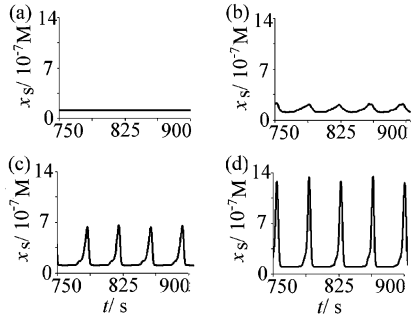

Figure 6. Simulated oscillations in the concentration of $HBrO_2$ in the surrounding solution, with an increasing number density of particles: (a) $n = 3000$ cm^{-3}, (b) 5000 cm^{-3}, (c) 9000 cm^{-3}, and (d) 11000 cm^{-3}. Parameters are listed in Table 3, row A.

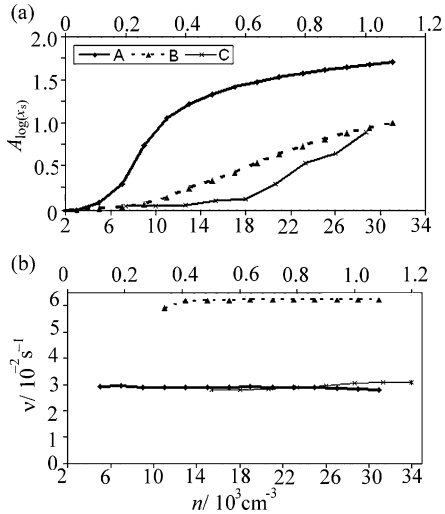

Figure 7. Simulated amplitude (a) and frequency (b) of oscillations as a function of the number density of particles with parameters listed in Table 3, rows A, B, and C (lower x-axis for A and B, upper x-axis for C).

The time series for x_s, the dimensionless concentration of $HBrO_2$ in the surrounding solution, is shown in Figure 6 for simulations with numerical parameter values listed in Table 3, row A. Oscillations in x_s appear for a number density of particles, n, greater than a certain amount. The appearance of oscillations can be distinguished from noise from a Fourier analysis of the data, and the values of n_{crit} and the corresponding frequency in x_s are listed in Table 2. The magnitude of oscillations is over a factor of 10 smaller than the oscillations in x_i on the individual particles. The amplitude, $A_{\log(x_s)}$, (taken from the average of five peaks in $\log(x_s)$ for comparison with experimental amplitudes in potential) and frequency of oscillations for the different experimental compositions A, B, and C are shown in Figure 7.

We also examined the frequency distribution and average amplitude of a subset of 10 000 oscillators from simulations with parameter values in Table 3, row A (Figures 8 and 9, respectively). With $n = 1000$ cm^{-3}, the mean frequency of 2.6×10^{-2} s^{-1} is slightly lower than that of the unstirred system.

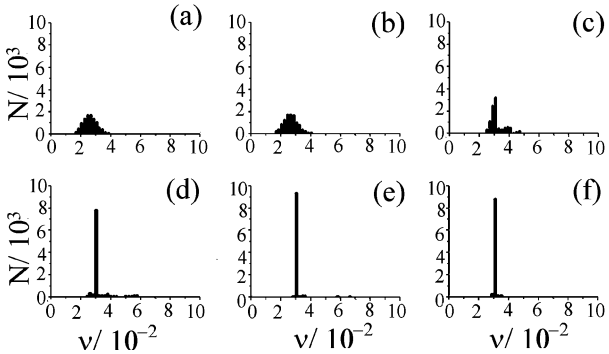

Figure 8. Simulated frequency distribution of 10 000 oscillators with an increasing number density of oscillators: (a) $n = 1000$ cm^{-3}, (b) $n = 3000$ cm^{-3}, (c) $n = 5000$ cm^{-3}, (d) $n = 7000$ cm^{-3}, (e) $n = 9000$ cm^{-3}, and (f) $n = 11\,000$ cm^{-3}. Parameters are listed in Table 3, row A.

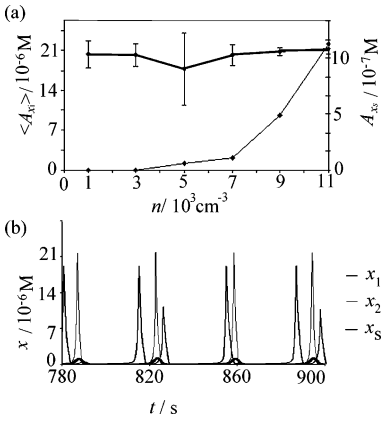

Figure 9. (a) Mean and standard deviation of the amplitude of $[HBrO_2]$ on 10 000 oscillators (upper data, left y-axis) compared with $[HBrO_2]$ in solution (lower data, right y-axis) as a function of the number density. (b) Temporal evolution of two oscillators x_1 and x_2 compared with temporal evolution of x_s for $n = 7000$ cm^{-3}. Parameters are listed in Table 3, row A.

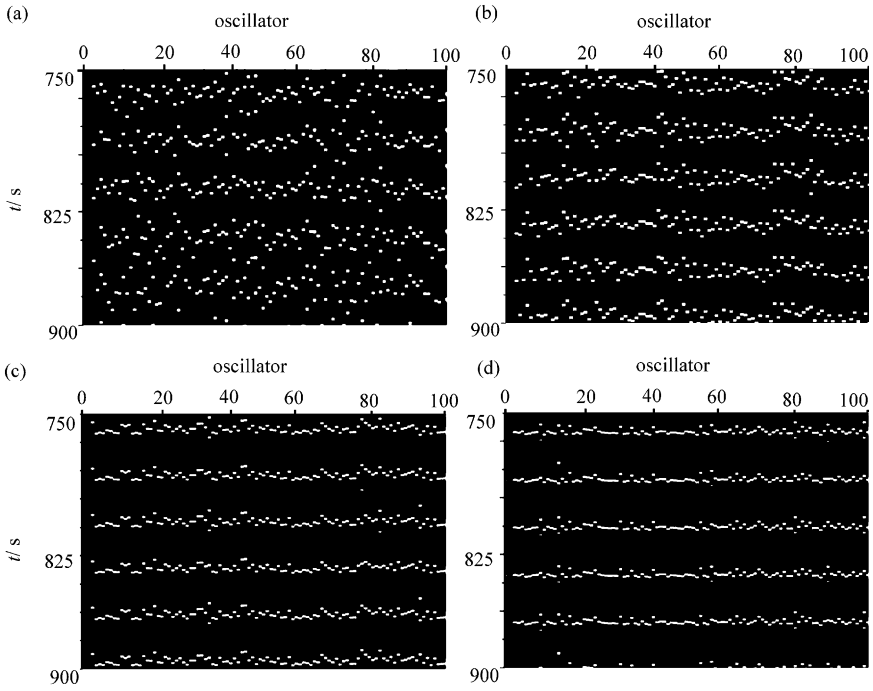

Figure 10. Simulated temporal evolution of a subgroup of 100 oscillators with an increasing number density: (a) $n = 5000$ cm^{-3}, (b) $n = 7000$ cm^{-3}, (c) $n = 9000$ cm^{-3}, and (d) $n = 11\,000$ cm^{-3}. The 0th oscillator corresponds to the mean field, that is, $\langle x_i \rangle / N$. Parameters are listed in Table 3, row A.

With $n = n_{crit} = 5000$ cm^{-3} (Figure 8c), there is the appearance of a coherent frequency at 3.0×10^{-2} s^{-1}. With $n = 7000$ cm^{-3}, 80% of the oscillators share the same frequency and this increases to 95% at 9000 cm^{-3} then decreases to 90% at 11 000 cm^{-3} (Figure 8f). The mean amplitude of the 10 000 oscillators $\langle A_{xi} \rangle$ (Figure 9a, upper curve) is constant for increasing n other than a slight decrease when $n = n_{crit}$. The standard deviation in the amplitude (vertical bars) decreases with increasing n. Thus the growth in amplitude of x_s (Figure 9a, lower curve) is not associated with a growth in the average amplitude of the individual oscillators. The response of the individual oscillators is shown in Figure 9b for two different oscillators and x_s. The oscillator x_2 shares the same frequency as x_s and has the same form as the oscillators in the uncoupled system. However, x_1 has a slightly higher frequency than x_s and displays a repeating pattern of two large amplitude peaks and then a smaller amplitude peak immediately after the bulk oscillation.

With the appearance of the common frequency at $n = 5000$ cm^{-3}, oscillators are phase-distributed, as illustrated in the oscillator−time plot in Figure 10a for 100 oscillators. With n increased to 7000 cm^{-3} (Figure 10b), those that share the same frequency begin to align in phase thus contributing to the mean field ($\langle x_i \rangle / N$, shown in the left-most column). More oscillators align for further increases in n (parts c and d of Figure 10), with a small fraction displaying the complex response similar to that of x_1 in Figure 9b.

Finally, we examine the transition for a higher value of k (= 20) with composition A and find that the nature of the transition changes dramatically. In this case, the large value of k means that the particles cease to oscillate for less than a critical number density of oscillators $n = 43\,000$ cm^{-3}, and the sudden appearance of oscillations in x_s (Figure 11a, upper curve) is associated with the appearance of oscillations on all particles (Figure 11a, lower curve). There is a small growth in the amplitude of x_s with increasing n. The form of the oscillations in x_s is the same as that of the individual oscillators (Figure 11b). The frequency of oscillations is significantly lower than

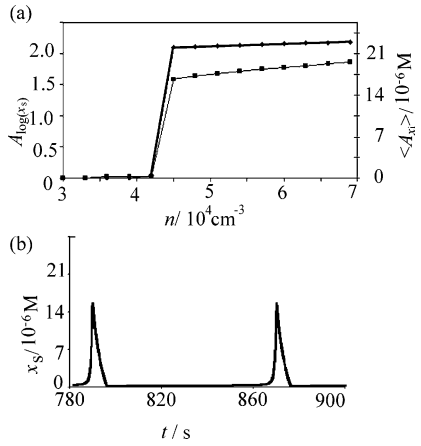

Figure 11. Simulations with high transfer coefficient ($k = 20$) and other parameters listed Table 3A. (a) Amplitude (upper curve, left y-axis) and average amplitude of 10 000 oscillators (lower curve, right y-axis) as a function of the number density of oscillators. (b) Temporal evolution of [$HBrO_2$] in the surrounding solution.

that of the uncoupled system ($\upsilon = 0.01$ s^{-1}) and decreases with increasing n.

Discussion and Conclusions

The purpose of this paper is the examination of the collective behavior of a population of relaxation oscillators in a well-stirred reactor, globally coupled through the exchange of chemicals with the surrounding solution. The oscillators consist of catalytic particles which display a range of frequencies when suspended in catalyst-free BZ solution. It has been proposed that a critical number density of oscillators is required for the observation of global oscillations in a number of cellular biological systems.[34] In our experiments, we observed the appearance of oscillations in the redox potential in the bulk solution for greater than a critical number density of particles n_{crit}. A simple model of the

experiment was constructed which includes the BZ reaction processes on each particle and the mass transfer of both the autocatalyst x and inhibitor y with the surrounding solution. The model qualitatively reproduces the dependence of the oscillatory amplitude on the initial concentrations and particle size and suggests that oscillations appear in the bulk solution when the particles partially synchronize. The growth in oscillatory amplitude is then associated with the phase alignment of oscillators. Particles that are not phase aligned become forced by the oscillations in the bulk solution.

The appearance of oscillations occurs for a slightly higher critical number density of particles (n_{crit}) in the system with the higher acid concentrations (B compared with A) as the particles themselves display higher average frequencies (Figure 1b), and hence lower average amplitudes, thus lowering their contribution of autocatalyst and inhibitor to the bulk solution and weakening the global coupling. The appearance of oscillations occurs for a much lower number of particles in system C with larger average particle size due to the increase in the factor V_i/V_s and hence reduced dilution of activator and inhibitor in solution, thus strengthening the magnitude of the global coupling. The distribution in experimentally observed amplitudes with n may result from the fact that coupled relaxation oscillators with large distributions in natural frequencies can have multiple entrainment states, and the macroscopic behavior observed then depends sensitively on the initial conditions.[35] Inhomogeneous mixing as well as uncertainty in the estimated number density of particles will contribute to this effect.

The frequencies of the bulk oscillations in the stirred solution correlate with the mean of the individual oscillators in both the experiments and the simulations for each of the different compositions. The fact that the mean frequency in the experiments is lower than the bulk frequency in each of the three cases might be a result of the small population size (150) used to construct the frequency distribution.

In the simulations, the transfer coefficient k was calculated from the scaling $\times\ k_{sl}A_i/V_i$, and the critical number density of particles n_{crit} for bulk oscillations matches the experimental results. The solid−liquid mass transfer coefficient k_{sl} increases with stirring rate[33] and hence the strength of the global coupling through the term $-k(x_i - x_s)$ will also increase, suggesting that a smaller n_{crit} is required for the observation of bulk oscillations with a fixed higher stirring rate. Preliminary experiments suggest that this is indeed the case. However, if the stirring rate is increased beyond a critical value, then $-k(x_i - x_s)$ becomes a drain on x_i and numerical investigations predict that all particles will cease to oscillate (Figure 11). In this case, the appearance of large amplitude oscillations occurs for a much higher n_{crit} and the frequency of oscillations is much lower than that of the uncoupled system. A full investigation of the affect of stirring rate on the appearance of oscillations will be reported elsewhere.

This system presents possibilities for the further characterization of the synchronization transition in systems of relaxation oscillators coupled through the concentrations of chemicals in an external solution. Future analysis of this system will include extraction of the order parameter from the global signal and characterization of the degree of phase synchronization.[36] Also we note that the transition depends on the value of the transfer coefficient k which depends on the particle size, and there is some variation in a typical sample of particles as purchased. This might be incorporated in the model, following a characterization of the distribution of particle surface area and volumes.

Acknowledgment. A.F.T. and R.T. would like to thank Silvia de Monte and Francesco d'Ovidio for experimental suggestions and useful discussion. This work was funded by EPSRC Grant No. GR/S09753/01.

Appendix 1. Model

The model is based on the ZBKE model for the ferroin-catalyzed BZ reaction with the concentration of bromide included explicitly for $i = 1,...,N$ particles

$$\frac{dX_i}{dt} = -k_2h_0X_iY_i + k_3h_0AY_i - 2k_4X_i^2 - k_5h_0AX_i + k_{-5}U_{ss}^2 + k_6U_{ss}(C - Z_i) - k_{-6}X_iZ_i - K(X_i - X_s)$$

$$\frac{dY_i}{dt} = -k_2h_0X_iY_i - k_3h_0AY_i + q\frac{k_7k_8BZ_i}{k_{-7}h_0(C - Z_i) + k_8} + k_9B - K(Y_i - Y_s)$$

$$\frac{dZ_i}{dt} = k_6U_{ss}(C - Z_i) - k_{-6}X_iZ_i - \frac{k_7k_8BZ_i}{k_{-7}h_0(C - Z_i) + k_8}$$

and in the surrounding solution

$$\frac{dX_s}{dt} = \frac{nV_i}{N}\sum_i^N K(X_i - X_s) - k_2h_0X_sY_s + k_3h_0AY_s - 2k_4X_s^2$$

$$\frac{dY_s}{dt} = \frac{nV_i}{N}\sum_i^N K(Y_i - Y_s) - k_2h_0X_sY_s - k_3h_0AY_s + k_9B$$

where the variables and parameter values are listed in Table 4

TABLE 4: Variables and Parameters in the Model

variables	
X_i	$[HBrO_2]_i$
Y_i	$[Br^-]_i$
Z_i	$[Fe(phen)_3^{3+}]_i$
U_i	$[HBrO_2^+]_i$
X_s	$[HBrO_2]_s$
Y_s	$[Br^-]_s$

parameters	values
A	$[HBrO_3]_0 = h_0[NaBrO_3]_0/(0.2 + h_0)$ M = 0.4 M
B	[BrMA] + [MA] = 0.14 M
C	catalyst = 1.7×10^{-3} M
h_0	acidity = 0.77 or 1.12 M
N	number of particles
q	stoichiometric factor (Table 2)
$k_2 - k_9$	see ref 30
n	number density of particles = N/V_s (units cm^{-3})
K	transfer coefficient = $k_{sl}A_i/V_i$ (units s^{-1})
k_{sl}	mass transfer coefficient = 0.01 cm s^{-1}
A_i	surface area of particle = 1.3×10^{-3} (1) or 1.5×10^{-2} (2) cm^2
V_i	reaction volume = 2×10^{-5} (1) or 9×10^{-4} (2) cm^3
V_s	volume of surrounding solution = 10 cm^3

and the value of U is obtained via its steady-state concentration

$$U_{ss} = \frac{1}{4k_{-5}}(k_6(C - z_i) + (k_6^2(C - z_i)^2 + 16k_{-5}k_5h_0Ax_i + 8k_{-5}k_{-6}x_iz_i)^{1/2})$$

The model is reduced to the dimensionless set of equations using the scalings given in Table 5.

TABLE 5: Scalings for the Dimensionless Model

variable	scaling
X	$k_5h_0Ax/2k_4$
Y	k_5Ay/k_2
Z	Cz
U	$(k_5h_0A)2u/2k_4k_6C$
t	$2k_4C\tau/(k_5h_0A)^2$
parameter	
ϵ_1	$k_5h_0A/2k_4C$
ϵ_2	$(k_5h_0A)^2/2k_4k_6C$
ϵ_3	$k_8/k_{-7}h_0C$
ϵ_4	k_5A/k_2C
α	$2k_4k_7k_8B/k_5^2k_{-7}h_0^3A^2$
β	$2k_4k_9B/(k_5h_0A)^2$
μ	$2k_3k_4/k_2k_5h_0$
γ	k_{-5}/k_6
δ	$k_{-6}C/k_5h_0A$
k	$2k_4CK/(k_5h_0A)^2$

References and Notes

(1) Winfree, A. T. *The Geometry of Biological Time*; Springer: New York, 1980.

(2) Pikovsky, A. S.; Rosenblum, M.; Kurths, J. *Synchronization: A universal concept in nonlinear sciences*; Cambridge University Press: Cambridge, U.K., 2001.

(3) Manrubia, S. C.; Mikhailov, A. S.; Zannette, D. H. *Emergence of Dynamical Order: Synchronization Phenomena in Complex Systems*; World Scientific Publishing Company: Singapore, 2004.

(4) Buck, J. *Q. Rev. Biol.* **1988**, *63*, 265

(5) Richard, P. *FEMS Microbiol. Rev.* **2003**, *27*, 547

(6) Glass, L. *Nature* **2001**, *410*, 277.

(7) Buzsaki, G.; Draguhn, A. *Science* **2004**, *304*, 1926

(8) Winfree, A. T. *J. Theor. Biol.* **1967**, *16*, 15.

(9) Kuramoto, Y. In *International Symposium on Mathematical Problems in Theoretical Physics, Lecture Notes in Physics*; Araki, H., Ed.; Springer: New York, 1975; Vol. 39, p 420.

(10) Nanjundiah, V. *Biophys. Chem.* **1998**, *72*, 1

(11) Dano, S.; Sorensen, P. G.; Hynne, F. *Nature* **1999**, *402*, 320.

(12) Dano, S.; Hynne, F.; De Monte, S.; d'Ovidio, F.; Sorensen, P. G.; Westerhoff, H. *Faraday Discuss.* **2001**, *120*, 261.

(13) Koppell, N.; Ermentrout, G. B. Mechanisms of phase-locking and frequency control in pairs of coupled neural oscillators. In *Handbook of Dynamical Systems: Toward applications*; Fiedler, B., Ed.; Elsevier: 2002; Vol. 2, p 3.

(14) Larter, R.; Speelman, B.; Worth, R. *Chaos* **1999**, *9*, 795.

(15) Gonze, D.; Bernard, S.; Waltermann, C.; Kramer, A.; Herzel, H. *Biophys. J.* **2005**, *89*, 120

(16) Weiner, J.; Holz, R.; Schneider, F. W.; Bareli, K. *J. Phys. Chem.* **1992**, *96*, 8915.

(17) Votrubova, V.; Hasal, P.; Schreiberova, L.; Marek, M. *J. Phys. Chem. A* **1998**, *102*, 1318.

(18) Crowley, M. F.; Field, R. J. *J. Phys. Chem.* **1986**, *90*, 1907.

(19) Crowley, M. F.; Epstein, I. R. *J. Phys. Chem.* **1989**, *93*, 2496.

(20) Vanag, V. K.; Yang, L. F.; Dolnik, M.; Zhabotinsky, A. M.; Epstein, I. R. *Nature* **2000**, *406*, 389.

(21) Von Oertzen, A.; Rotermund, H. H.; Mikhailov, A. S.; Ertl, G. *J. Phys. Chem. B* **2000**, *104*, 3155.

(22) Kiss, I. Z.; Zhai, Y.; Hudson, J. L. *Science* **2002**, *296*, 1676.

(23) Kiss, I. Z.; Wang, W.; Hudson, J. L. *J. Phys. Chem. B* **1999**, *103*, 11433.

(24) Kiss, I. Z.; Gaspar, V.; Hudson, J. L. *J. Phys. Chem. B* **2000**, *104*, 7554.

(25) Zhai, Y.; Kiss, I. Z.; Hudson, J. L. *Ind. Eng. Chem. Res.* **2004**, *43*, 315.

(26) Mikhailov, A. S.; Zanette, D. H.; Zhai, Y.; Kiss, I. Z.; Hudson, J. L. *Proc. Natl. Acad. Sci. U.S.A.* **2004**, *101*, 10890.

(27) Strogatz, S. H. *Physica D* **2000**, *143*, 1.

(28) Yoshikawa, K.; Aihara, R.; Agladze, K. *J. Phys. Chem. A* **1998**, *102*, 7649.

(29) Maselko, J.; Reckley, J. S.; Showalter, K. *J. Phys. Chem.* **1989**, *93*, 2774.

(30) Nugent, C. R.; Quarles, W. M.; Somomon, T. H. *Phys. Rev. Lett.* **2004**, *93*, 218301.

(31) Neufeld, Z.; Kiss, I. Z.; Zhou, C.; Kurths, J. *Phys. Rev. Lett.* **2003**, *91*, 84101.

(32) Zhabotinsky, A. M.; Buchholtz, F.; Kiyatkin, A. B.; Epstein, I. R. *J. Phys. Chem.* **1993**, *97*, 7578.

(33) Pangarkar, V. G.; Yawalkar, A. A.; Sharma, M. M.; Beenackers, A. A. C. M. *Ind. Eng. Chem. Res.* **2002**, *41*, 4141.

(34) Aldridge, J.; Pye, E. K. *Nature* **1979**, *259*, 670.

(35) Daido, H. *Phys. Rev. Lett.* **1996**, *77*, 1406.

(36) Zhai, Y.; Kiss, I. Z.; Daido, H.; Hudson, J. L. *Physica D* **2004**, *199*, 387.